# Micromachined Thick Mesh Filters for Millimeter-Wave and Terahertz Applications

Yi Wang, *Senior Member, IEEE*, Bin Yang, Yingtao Tian, Robert S. Donnan, and Michael J. Lancaster, *Senior Member, IEEE*

***Abstract*—This paper presents several freestanding bandpass mesh filters fabricated using an SU-8-based micromachining technique. The important geometric feature of the filters, which SU8 is able to increase, is the thickness of the cross-shaped micromachined slots. This is five times its width. This thickness offers an extra degree of control over the resonance characteristics. The large thickness not only strengthens the structures, but also enhances the resonance quality factor ($Q$-factor). A 0.3-mm-thick, single-layer, mesh filter resonant at 300 GHz has been designed and fabricated and its performance verified. The measured $Q$-factor is 16.3 and the insertion loss is 0.98 dB. Two multi-layer filter structures have also been demonstrated. The first one is a stacked structure of two single mesh filters producing a double thickness, which achieved a further increased $Q$-factor of 27. This is over six times higher than a thin mesh filter. The second multi-layer filter is an electromagnetically coupled structure forming a two-pole filter. The coupling characteristics are discussed based on experimental and simulation results. These thick mesh filters can potentially be used for sensing and material characterization at millimeter-wave and terahertz frequencies.**

***Index Terms*—Filters, frequency-selective surfaces (FSSs), micromachining, millimeter-wave (mm-wave) devices.**

## I. Introduction

A MESH filter is an important frequency-selective component in many millimeter-wave (mm-wave) and terahertz (THz) systems. It is also known as a frequency-selective surface (FSS). Mesh filters have been widely used as filters, beam splitters, reflectors, and as special electromagnetic boundaries [1]. In the past few years, bandpass and bandstop mesh filters have also been used as resonators for sensing purposes [2], [3]. It is worth noting that the mesh filter is traditionally called a "filter." However, essentially, a single mesh filter can be treated as a resonator. It has been shown that different formations, binding states, or concentrations of some important biomolecules exhibit different refraction index and absorption coefficients at THz frequencies. Thus, when the resonator is loaded with the material of concern, its resonance frequency shifts and resonance quality factor ($Q$-factor) changes depending on the complex permittivity of the material. For instance, the dielectric properties of single- and double-stranded DNA can be distinguished in this way [2]. The FSS has also been used to characterize liquid crystals at mm-wave frequencies [4]. Resonant structures have been widely used at microwave frequencies for material characterization. With the increasing demand for knowledge of material properties at THz frequencies [5]–[10] from device and system engineers, it is anticipated that more THz resonator techniques will emerge. Compared with time-domain spectroscopy (TDS), resonator-based techniques, when coupled with frequency-domain network analysis, offer higher sensitivity and frequency resolution. Although this is a band-limited technique, it is able to increase the sensitivity to binding states of DNA by 1000 times over TDS and to detect material quantities on the order of femtomoles [11], [12]. The high sensitivity comes from the increased interaction length, time, and power density as the sample is exposed to oscillating and enhanced THz waves within the confined regions of the resonators. The detection sensitivity depends on the $Q$-factor of the resonator as well as the interaction region between the electromagnetic fields and materials [13]. $Q$-factors quantify the sharpness of resonance curves in the frequency domain. A sharper curve enables the detection of smaller changes of the resonance frequency.

A mesh filter is a popular choice for free-space applications. Most existing mesh filters are made from thin metal wires or sheets or patterned thin films on substrates such as silicon or polymers. Usually the thickness of metal mesh structures is very small compared with wavelength and dimensions of the patterned features, so the fringe fields beyond the mesh surface can be significant. The loaded $Q$-factor of a mesh filter is generally very low. Melo *et al.* [14] reviewed 19 cross-shaped mesh filters (bandpass) ranging from 138 GHz to 14 THz all with $Q$-factors less than 7.3. In [15], a cross-shaped mesh filter on glass substrate exhibited a $Q$-factor of 7.5 at 480 GHz, whereas the filter used for DNA sensing [3] had a $Q$-factor of only 1.1 at 0.8 THz. In this work, a thick mesh filter has been developed; the thickness of the mesh filter is over a quarter of a wavelength, nearly

Manuscript received September 29, 2013; revised November 19, 2013; accepted December 10, 2013. Date of publication January 09, 2014; date of current version March 04, 2014 This work was supported by the University of Greenwich Research and Enterprise Investment Programme 2012/13 and the U.K. Engineering and Physical Sciences Research Council under Contract EP/I014845/1 and Contract EP/H029656/1.

Y. Wang is with the Department of Electronic Electrical Computer Engineering, University of Greenwich, Chatham Maritime, Kent, ME4 4TB, U.K. (e-mail: yi.wang@gre.ac.uk).

B. Yang was with the School of Electronic Engineering and Computer Science, Queen Mary University of London, London, E1 4NS U.K. He is now with the Engineering, Sports and Science Academic Group, University of Bolton, Bolton, BL3 5AB, U.K.

Y. Tian and M. J. Lancaster are with the School of Electronic Electrical Computer Engineering, University of Birmingham, Edgbaston, Birmingham B15 2TT, U.K.

R. S. Donnan is with the School of Electronic Engineering and Computer Science, Queen Mary University of London, London, E1 4NS, U.K.

Color versions of one or more of the figures in this paper are available online at http://ieeexplore.ieee.org.

Digital Object Identifier 10.1109/TTHZ.2013.2296564

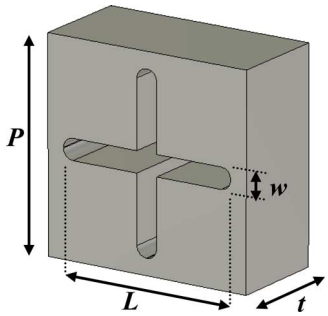


Fig. 1. Diagram of one unit cell of the mesh filter with cross-shaped slots.

five times the slot width. This essentially introduces guided regions in the slots and transforms the mesh filter from a surface structure to a volumetric one. By doing so, fringe fields are suppressed, more electromagnetic fields concentrate within the slots and the $Q$-factor is significantly enhanced.

Thin-film photolithography is not capable of forming such a thick structure. Bulk micromachining techniques have to be resorted to. Previously, a freestanding FSS of 12.5-$\mu$m thickness and with a smallest line feature of 20 $\mu$m was fabricated by silicon deep reactive ion etching (DRIE) [16]. An even thicker THz mesh filter of 2 mm in depth, 25 times the slot-width, was fabricated using X-ray LIGA [17]. In both cases, the purpose for introducing the thickness was to enhance mechanical strength. This paper, however, focuses on the electromagnetic characteristics and advantages that thickness engenders. The thick mesh filter is fabricated using a micromachining technique based on thick photoresist SU-8. This is a simple and potentially low-cost fabrication method and yet provides better surface quality of the structure than laser or DRIE based methods. The technique has been successfully used to produce mm-wave 3-D air-filled devices of more complicated structures [18].

## II. Design

Fig. 1 shows one unit-cell of the mesh filter with cross-shaped slots. The critical dimensions are the period $P$ of the cells, the length $L$ of the cross, the width $w$ of the slot, and the thickness $t$. $P = 0.625$ mm and $w = 0.0625$ mm are fixed in this study. The fundamental resonant frequency of the cell is mainly determined by $L$. For a chosen thickness $t$, $L$ is adjusted so that the mesh filter resonates at 300 GHz. The resonance shifts upwards by 1.9% with $t$ increasing from 0.01 to 0.10 mm, and by 0.9% from 0.1 to 0.3 mm. This can be seen from Fig. 2, where $L$ has to be increased in order to keep the resonance at 300 GHz. When $t$ is over 0.3 mm, this increasing trend becomes negligible, and the resonance frequency is no longer sensitive to the thickness. However, the loaded $Q$-factor increases linearly with the thickness. This thickness-enhanced $Q$-factor was the main motivation of this work. For a 0.3 mm $(0.3\lambda_0)$ thick mesh filter resonant at 300 GHz, the length $L$ is found to be 0.527 mm by full-wave simulations [19]. This is in good agreement with the calculated value of 0.531 mm from the empirical formula derived by Möller *et al.* [20].

The mesh filter is essentially a resonant structure interacting with plane waves. Its equivalent circuit can be represented by

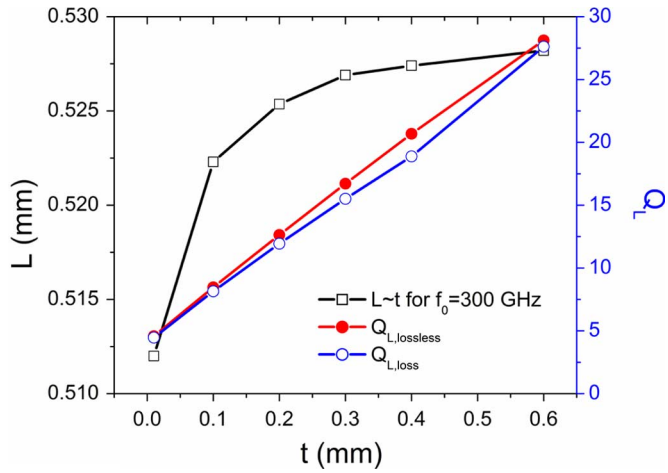


Fig. 2. Relationship between the thickness $t$ of the mesh and the length $L$ of the cross for a 300-GHz mesh filter. It also shows the increase of the loaded $Q$-factor $Q_L$ with the thickness.

Fig. 3(a). The resistance $R_{\text{ext}}$ is to quantify the coupling (or external $Q$-factor, $Q_{\text{ext}}$) between plane waves and the periodic mesh structure, which is represented by a parallel resonant circuit with an unloaded $Q$-factor of $Q_u$. In the full-wave simulations, if no loss is considered, the simulated $Q$-factor $Q_{L,1}^{-1} = 2 \times Q_{\text{ext}}^{-1}$, as $Q_u$ tends to be infinite. If the conductor loss is considered (no dielectric loss is involved in this structure, which is an advantage), a different loaded Q-value can be found, i.e., $Q_{L,2}^{-1} = 2 \times Q_{\text{ext}}^{-1} + Q_u^{-1}$. Here, a 1.5-$\mu$m-thick silver coating with a surface roughness of 200 nm is assumed as a worst case scenario, and a simple frequency-dependent surface-impedance model is used (nine points between 280–320 GHz with a surface resistance of 0.254 $\Omega$ at 300 GHz) in the simulation. Then, the unloaded $Q$-factor $Q_u$ can be extracted from these two equations. For the 0.3-mm-thick mesh filter, the simulated $Q$-factors are $Q_{L,1} = 16.7$ and $Q_{L,2} = 15.5$, so $Q_u$ is estimated to be 216. $Q_u$ is not sensitive to the thickness of the mesh filter whereas the loaded $Q$-factors increase linearly with thickness as shown in Fig. 2. For a "thin" structure (e.g., $t = 0.01$ mm $= 0.01\lambda_0$), the $Q_L$ is only 4.46. This is increased by over sixfold to 27.6 when $t = 0.6$ mm $= 0.6\lambda_0$. This significant enhancement is a result of more average energy stored within the guided region of the slots introduced by the sheer thickness of the mesh structure.

It should be noted that there are other methods that can be used on top of the thickness to increase the $Q$-factor of a single mesh filter. Increasing the inter-element spacing $P$ reduces the resonance bandwidth but at the cost of reduced transmission efficiency and increased side lobes. Oblique incidence could result in a reduced bandwidth [1]. Introducing transmission zeros near the resonance can also sharpen the roll-off. Although this can be more effective than the previous two methods, it requires two interfering transmission paths through the mesh filter which often involves more complicated cell structure [21]. Combining the thickness with all or some of these methods can increase the $Q$-factor by an order of magnitude or more. This paper only focuses on the effect of the thickness.

The above-mentioned resonance in the cross-shaped structure is related to the dipole-type of resonance along the slot

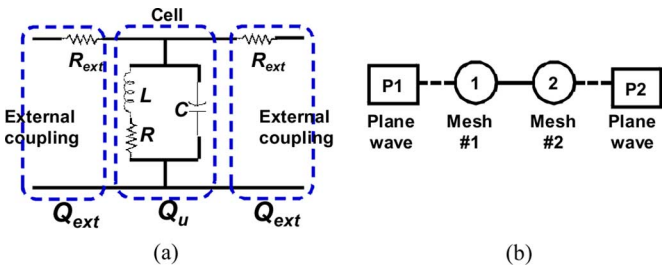


Fig. 3. (a) Equivalent circuit of the cross-shaped mesh filter. $R_{\rm ext}$ and $Q_{\rm ext}$ are related to the coupling between the resonator and the input/output plane waves. The resonance is represented by the parallel LCR circuit with an unloaded $Q$-factor of $Q_u$. (b) Coupling topology of a two-pole mesh filter, where "1" and "2" denote the resonators (individual mesh filters) and "P1" and "P2" are the ports (plane waves in this case).

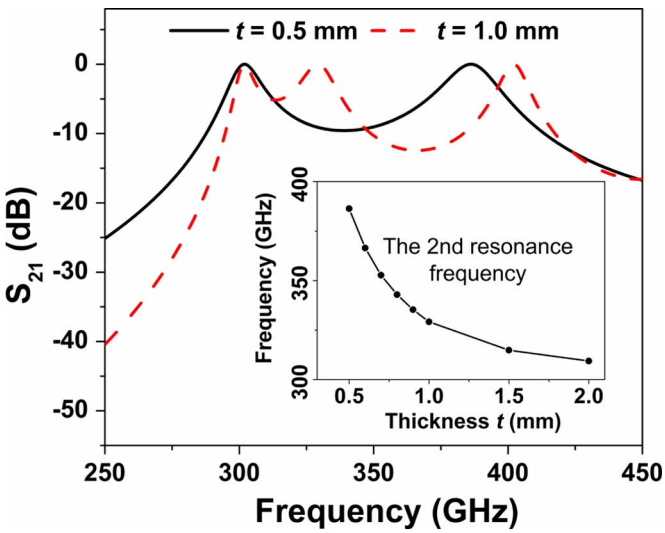


Fig. 4. Simulated transmission responses of the mesh filters with $t = 0.5$ and 1.0 mm, respectively, over a broad frequency range. (Inset) Change of the 2nd resonance frequency (thickness peak) with the thickness.

[1]. The thickness of the mesh filter brings about another resonance related to the waveguide mode in the guided channels. The horizontal or vertical channels can be approximated by a rectangular waveguide with a width of $L = 0.527$ mm and a height of $w = 0.0625$ mm. Its $\rm TE_{10}$ cutoff frequency is therefore 285 GHz. Thus, when the depth of the channel approaches half of the guided wavelength, the $\rm TE_{101}$ mode resonates. This resonance frequency has a more prominent dependency on the thickness, as can be seen from the simulated transmission responses in Fig. 4. The inset shows the change of this second resonance with thickness exhibiting a nonlinear relation, which is a signature of waveguide modes. This resonance has been referred to as "thickness peak" in [22]. When the thickness of the mesh filter is over a quarter of a wavelength, the fundamental resonance barely changes whereas the thickness peak shifts to lower frequency. The two resonances eventually become degenerate. The closing-in of the "thickness peak" would broaden the resonance and reduce the $Q$-factor. To overcome this, transmission zeros may be introduced in proximity of the resonance peak in the frequency domain.

## III. Fabrication

The core material of the structure is SU-8-50 which is completely metalized to form the mesh filter. SU-8 is a thick photoresist sensitive to UV light and can be used to form 3-D structures up to about 2 mm thick [23]. The process starts with spin coating SU-8-50 on a 100 mm silicon wafer. The thickness of the SU-8 layer was controlled by the weight. In this case, 3.6 g SU-8 was applied to achieve the required 0.30-mm thickness, as derived from previous calibrations. The edge bead was removed to improve uniformity. The SU-8 covered wafer was then placed on a leveled stage (with a tolerance of 0.1°) for several hours for planarization. After that, the wafer was baked at 65°C for 30 min and then at 95 °C for 165 min. A slow temperature ramp was used during the heat-up and cool-down to minimize the residual stress in SU-8. Once the wafer was cooled down after the soft-bake, it was exposed in a Cannon PLA-501 mask aligner. Typically, the light coming out of the UV lamp consists of three main lines at 365, 405, and 436 nm. It is known that long wavelength UV light can penetrate deeper into the SU-8 but is less effective in inducing photo acid for cross-linking. So the wafer was first exposed for $2 \times 40$ s with a L39 filter, only letting through lines above 400 nm to achieve deep penetration. Next, a PL360 filter was used to allow the wafer to be exposed to the i-line at 365 nm for another $2 \times 40$ s. A 2-min interval was introduced between each 40-s exposure to avoid over-heating and to stabilize the photoresist. A post-exposure bake was then conducted at 70 °C for 45 min to form sufficient cross-linking with relatively low residual stress. The unexposed SU-8 was removed by developing in EC solvent (supplied by Dow Chemical Company) for 25 min, assisted by vigorous magnetic stirring agitation. To make the structure durable, it was hard-baked at 95 °C for 15 min. The patterned structure was then released from the wafer by soaking in 10% NaOH solution for a few hours. Finally, the released SU-8 structure was cleaned under oxygen plasma for 30 s and metalized with silver using a Cressington 308R metal evaporator. A 50-nm chrome adhesion layer was deposited before 1.5–2.0-$\mu$m-thick silver was evaporated onto all surfaces. This should be sufficient to avoid the skin-effect problem at 300 GHz. The end corners of the cross-shaped slots were rounded to a radius of 0.03 mm in order to further relieve stress induced in SU-8 during thermal cycling. This also reduces the current density in a beneficial way. The ratio between the thickness and the slot width of the fabricated mesh filters is 5:1. This ratio is only limited by the evaporation method used here. It is a line-of-sight deposition technique. A trench too deep will prevent sufficient materials from being deposited onto the sidewalls. To metalize structures with a higher aspect ratio, diffusive sputtering technique can be used instead. It is also possible to thicken up the mesh structure by using a more complicated multiple SU-8 deposition process [18]. Alternatively, two metalized mesh filters can be stacked on top of each other. Experimental results from such a stacked configuration will be presented later.

## IV. Measurement

The mesh filters were measured in a free space quasi-optical (QO) system driven by a vector network analyzer. A trans-

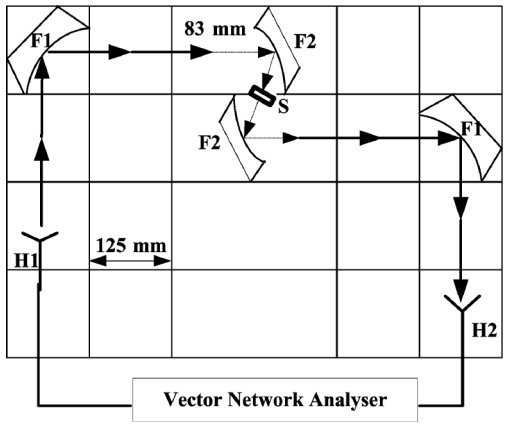


Fig. 5. Schematic diagram of the transmissometer. H1 and H2 denote the corrugated feed-horns; F1 is an ellipsoidal reflector with a focal length of 250 mm; F2 is a spherical mirror with a focal length of 83 mm; S is the device under test.

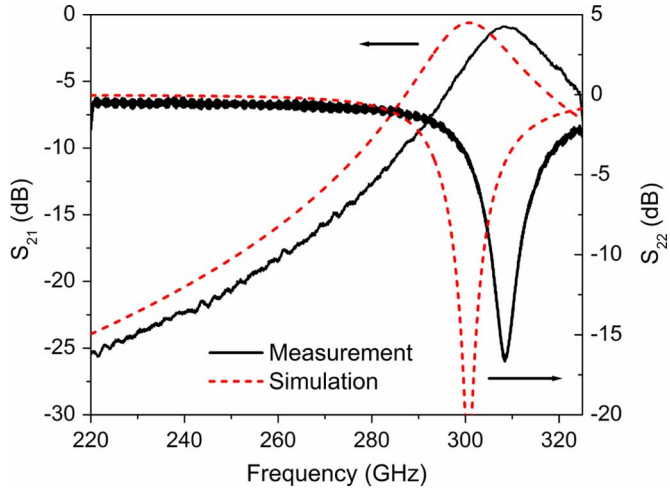


Fig. 6. Measured transmission ($S_{21}$) and reflection ($S_{22}$) responses of the mesh filter in comparison with the simulations.

missometer configuration as shown in Fig. 5 was used to measure the transmission coefficient $S_{21}$. The QO circuit can serve frequencies from 110 GHz up to 1 THz. A shaped corrugated feed horn H1 was used to transform waveguide modes from the mm-wave extension head to linearly polarized Gaussian beams in free space. An ellipsoidal reflector F1 receives the signal-beam diverging from the horn and transforms it into a linearly-polarized quasi-collimated beam. This is subsequently focused by a fast spherical mirror F2 and passes through the device under test (DUT). A similar fast spherical mirror and ellipsoidal reflector condense the transmitted beam into the feed-horn receiver of another VNA extension head unit. The plane-wave angular-spectrum of the beam incident on the DUT is Gaussian in form with a small width-parameter of only 1° at 110 GHz. In all cases, the beam is at normal incidence with its TE polarization aligned to the vertical slots of the mesh filters.

In this paper, the measurement band is limited to 220–325 GHz by the WR-3 waveguide extension heads. The beam spot radius is 1.25 mm over the band. The DUT is 12 mm × 15 mm in size with a mesh area of 9 mm × 9 mm. The small beam spot therefore regards the sample as a large plane surface so that edge-diffraction effects are not considered. The transmission measurement was calibrated by a 'thru' response providing a dynamic range of 60 dB. A reflectometer configuration, similar to that demonstrated in [24], was used to measure the reflection coefficients $S_{11}$ and $S_{22}$. The calibration was performed on a reference metal-plate reflector at the position of the DUT. The dynamic range was 55 dB.

Fig. 6 shows the measured and simulated responses of the mesh filter. Table I compares their resonant frequencies, $Q$-factors, and minimum insertion losses. The $Q$-factors agree closely; to within 4.3%. The measured resonant frequency is 2.5% higher. This is caused by fabrication tolerances mainly from two factors. First is the thickness of the SU-8 base material. However, as discussed earlier, the resonant frequency is not very sensitive to this. In the worst case scenario, assuming a thickness inaccuracy of ±20 $\mu$m, the frequency would have been shifted by only 0.2 GHz. The second factor is the sidewall slope of thick SU-8 structures. As the thickness increases, it becomes increasingly difficult for the UV to penetrate into

TABLE I
COMPARISON BETWEEN MEASUREMENT AND SIMULATION

| | Loaded Q-factor | Resonant frequency (GHz) | Insertion loss (dB) |
|---|---|---|---|
| Simulation | 15.6 | 300.8 | -0.61 |
| Measurement | 16.3 | 308.2 | -0.98 |

The parameters used in the simulation model and photolithography mask are: $P$ = 0.625 mm, $w$ = 0.0625 mm, $L$ = 0.525 mm.

the lower part of the SU-8 layer. Therefore, the dimensions of the slots in the upper part the SU-8, facing UV, are defined more accurately than those in the lower part. This produces narrowing channels with non-vertical walls, which effectively reduces the length of the cross-aperture and increases the resonant frequency. The narrowing channel also increases the $Q$-factor slightly. To account for the full frequency discrepancy between simulation and measurement, a deviation of 2.5° from vertical would be expected according to full-wave modeling. A simple optical measurement of the DUT indicated the deviation was around 1.9°.

As mentioned earlier, one way to further increase the thickness of the mesh filter is to stack two mesh filters on top of each other, effectively making a 0.6-mm-thick structure. The effect of doing this can be seen from Fig. 7. The resonance curve becomes sharper indicating an increased $Q$-factor, measured to be 27. This is consistent with the simulated $Q$-factor of 28 when $t$ = 0.6 mm. However, the measured insertion loss is 4.3 dB, which is significantly higher than the predicted 1.0 dB. This extra loss is most likely to be due to contact gap and misalignment between the two meshes. This assembly error can be mitigated in future by applying micro-alignment procedures.

When two mesh filters are placed in proximity to each other, electromagnetic coupling between them occurs. With a proper control of the coupling level, a two-pole filter can be realized. Such a coupling structure can be represented by Fig. 3(b), analogous to resonator-coupled microwave filters [25]. The main difference lies in that here plane waves, rather than guided waves, are coupled to and through the two resonators. The bandwidth and matching of the passband can be adjusted to some extent by altering the distance between the two mesh filters. Applying

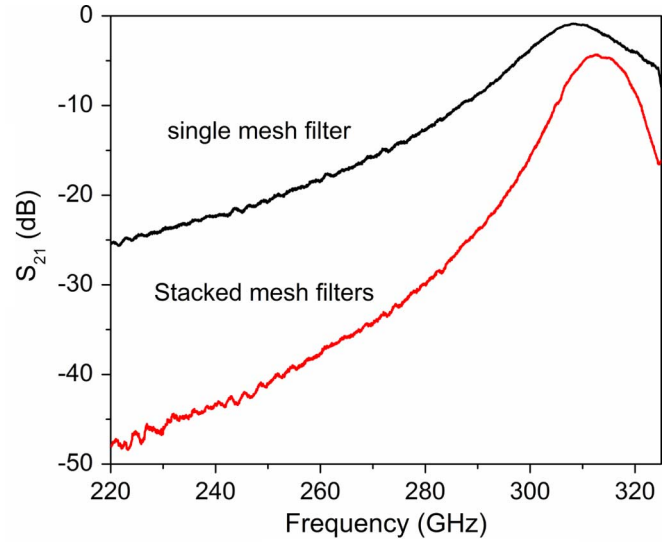


Fig. 7. Measured transmission responses of two mesh filters stacked together, in comparison with a single mesh filter.

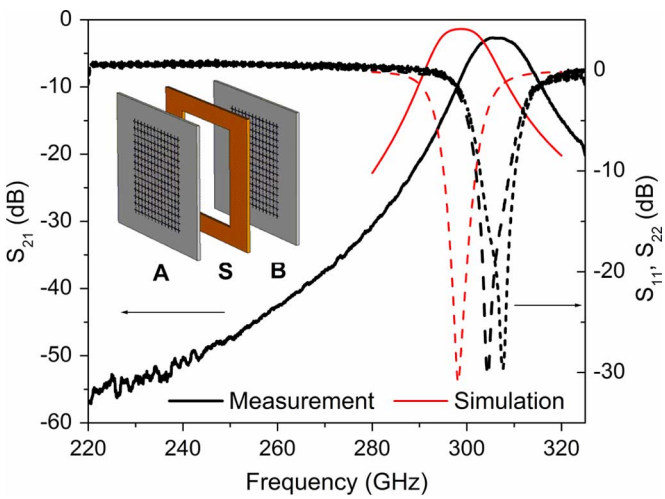


Fig. 8. Transmission and reflection responses of a two-pole mesh filter. Inset: Exploded view. A and B: mesh filter-1 and -2; S: SU-8 based spacer.

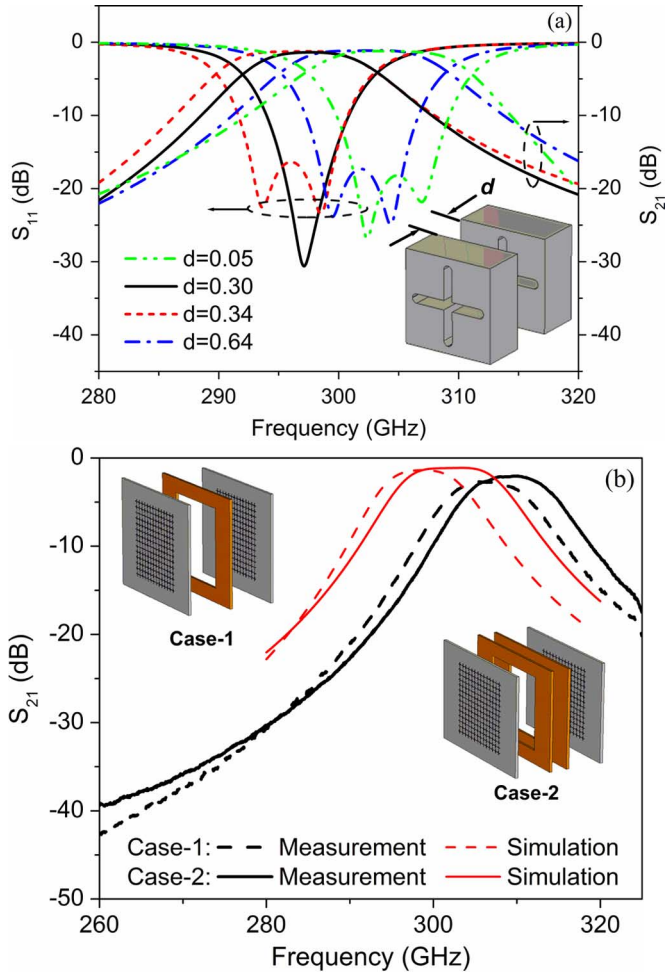


Fig. 9. (a) Simulated passband responses with different separations $d$ (in millimeters) between the two mesh filters. (b) Measurement results for $d = 0.3$ mm (Case-1 using one spacer as in Fig. 8) and $d = 0.6$ mm (Case-2 using two spacers).

dielectric overlays is another effective way of shaping the passband characteristics [1].

The two-pole, coupled-mesh filter set, was devised as illustrated by the inset of Fig. 8. The two mesh filters are separated by a 0.30-mm-thick spacer formed of bare SU-8. This triple-layer assembly was clamped together using a sample holder for measurements. Its performance was successfully verified as shown in Fig. 8. The frequency shift is attributed to the slight de-tuning of the individual mesh filter as mentioned earlier. Since the two mesh structures (A and B) are not identical due to fabrication tolerance, the measured $S_{11}$ and $S_{22}$ are slightly different. By adjusting the separation between the two mesh filters, the bandwidth and matching of the two-pole filter can be changed and optimized. For example, in Fig. 9(a), by increasing the separation $d$ from 0.30 mm (the case of Fig. 8) to 0.34 mm, the bandwidth is increased and two distinct reflection zeros appear. Another similar matching condition can be realized at a much larger separation of 0.64 mm, i.e., $0.64\lambda_0$. This is not possible for conventional single-element resonators, as the coupling (usually through evanescent wave modes) would drop rapidly with distance. In the case of the periodic mesh structure, the transmitted wave through one mesh filter keeps its planar wave-front and does not decay much. So the coupling level can be restored at intervals as in transmission lines. For the same reason with regard to plane wave interaction, the couplings in the triple-layer structures are not sensitive to misalignment between the two mesh filters. This is an advantage over evanescent-coupling-based filters, such as waveguide cavity filters. When the two mesh filters are in very close proximity, e.g., $d = 0.05$ mm, a third matching condition can be met as shown in Fig. 9(a).Now $d$ is comparable to the slot width, so the coupling should be attributed to evanescent modes of the mesh filter. Practically, this condition is not very useful because of its sensitivity to the distance between the meshes. Finally, Fig. 9(b) compares two cases with different separations between mesh filters. Case-1 is the device in Fig. 8, whereas Case-2 used two spacers to separate the mesh filters by, nominally, $d = 0.6$ mm. Their performances are experimentally verified.

## V. Discussion and Conclusion

This paper reported several free-space bandpass filters based on a thick mesh filter structure and fabricated using SU-8 micromachining techniques. The increased thickness is the key feature of the mesh filter, with a thickness-to-slot ratio of 5. This thickness is a new degree of freedom in shaping the resonance characteristics. The loaded $Q$-factors of the mesh filter increase linearly with thickness. The enhanced $Q$-factor potentially provides higher sensitivity and frequency resolution when used to characterize materials or as a resonator-based sensor. Apart from the fundamental resonance of a normal mesh filter, the thick structure accommodates another almost independent resonance of the waveguide-mode nature—the so-called thickness peak. This feature may be explored for multifrequency material characterization.

Although the SU-8 material can be used to form structures as thick as 2 mm, the achievable thickness of the single layer mesh filter in this work is limited by the line-of-sight evaporation method used. Sputtering can overcome this limitation. A thicker structure has been formed by stacking two individually made filters. Further increase in $Q$-factor has been achieved. The challenge in this case is to improve the contact and alignment between layers. By properly coupling (or cascading [1]) two mesh filters together, controllable passband characteristics (bandwidth and matching) have been demonstrated. It has also been shown that matching conditions can be realized at vastly different separations from close proximity of 0.05 mm to over half a wavelength, at $0.64\lambda_0$. The advantage of coupling via plane waves over a relatively large separation is its low sensitivity to misalignment.

All of the above-mentioned configurations of mesh filters have been experimentally verified, and good agreements have been achieved between the measurements and designs. The 2.5% discrepancy in resonant frequencies can be largely attributed to the sidewall slope. For the single mesh filter and the two-pole filters, the slightly higher insertion losses are conductor losses not accounted for. For the stacked filters, the contact and alignment problems have caused significantly higher loss than the predicted.

The presented mesh filters have achieved high $Q$-factors of 16.3 with a thickness of 0.3 mm and 27 with a thickness of 0.6 mm at 300 GHz. This is significantly higher than for a thin mesh filter, and compares favorably with those in [14], [15] which demonstrated Q-factors of less than 7.5 from 138 GHz up to 1 THz. The $Q$-factor is not only enhanced by the useful thickness, but also by the elimination of dielectric losses. The increased $Q$-factor of the thick mesh filter can be enhanced further by combining with other techniques, promising to achieve orders of magnitude increase. The thick mesh filter designs demonstrated here can be scaled to terahertz frequencies for potential applications such as sensing and material characterizations. This resonator-based frequency-domain techniques may become a useful complement to existing time-domain techniques.

## Acknowledgment

Y. Wang would like to thank S. Martin and C. Ryder, University of Greenwich, for technical support.

## References

[1] B. A. Munk, *Frequency Selective Surfaces*. New York, NY, USA: Wiley, 2000.

[2] H. Yoshida, Y. Ogawa, Y. Kawai, S. Hayashi, A. Hayashi, C. Otani, E. Kato, and F. Miyamaru, "Terahertz sensing method for protein detection using a thin metallic mesh," *Appl. Phys. Lett.*, vol. 91, Dec. 2007, Art. ID 253901.

[3] T. Hasebe, S. Kawabe, H. Matsui, and H. Tabata, "Metallic mesh-based terahertz biosensing of single- and double-stranded DNA," *J. Appl. Phys.*, vol. 112, Nov. 2012, Art. ID 094702.

[4] R. Dickie, P. Baine, R. Cahill, E. Doumanis, G. Goussetis, S. Christie, N. Mitchell, V. Fusco, D. Linton, J. Encinar, R. Dudley, D. Hindley, M. Naftaly, M. Arrebola, and G. Toso, "Electrical characterisation of liquid crystals at millimetre wavelengths using frequency selective surfaces," *Electron. Lett.*, vol. 48, no. 11, pp. 611–612, May 2012.

[5] N. Hiromoto, Y. Okita, and I. Hosako, "Measurement of terahertz properties of pastes and gels used in medical examinations," in *Proc. Int. Conf. Infr. Milli. Waves Int. Conf. Tera. Electron.*, Sep. 2007, pp. 559–560.

[6] J. A. Hejase, O. R. Paladhi, and P. Chahal, "Terahertz characterization of dielectric substrates for component design and nondestructive evaluation of packages," *IEEE Trans. Compon. Packag. Manuf. Technol.*, vol. 1, no. 11, pp. 1685–1694, Nov. 2011.

[7] B. B. Yang, S. L. Katz, K. L. Willis, M. J. Weber, I. Knezevic, S. C. Hagness, and J. H. Booske, "A high-Q terahertz resonator for the measurement of electronic properties of conductors and low-loss dielectrics," *IEEE Trans. THz Sci. Technol.*, vol. 2, no. 4, pp. 449–459, Jul. 2012.

[8] M. N. Afsar, A. Bellemans, J. R. Birch, G. W. Chantry, R. N. Clarke, R. J. Cook, R. Finsy, O. Gottman, J. Goulon, R. G. Jones, U. Kaatze, E. Kestemont, H. Kilp, M. Mandel, R. Pottel, J.-L. Rivail, C. B. Rosenberg, and R. Van Loon, "A comparison of dielectric measurement methods for liquids in the frequency range 1 GHz to 4 THz," *IEEE Trans. Instrum. Meas.*, vol. 29, no. 4, pp. 283–288, Dec. 1980.

[9] V. V. Parshin, M. Y. Tretyakov, M. A. Koshelev, and E. A. Serov, "Modern resonator spectroscopy at submillimeter wavelengths," *IEEE Sensors J.*, vol. 13, no. 1, pp. 18–23, Jan. 2013.

[10] A. G. Markelza, A. Roitbergb, and E. J. Heilweila, "Pulsed terahertz spectroscopy of DNA, bovine serum albumin and collagen between 0.1 and 2.0 THz," *Chem. Phys. Lett.*, vol. 320, no. 1–2, pp. 42–48, Mar. 2000.

[11] M. Nagel, P. H. Bolivar, M. Brucherseifer, H. Kurz, A. Bosserhoff, and R. Büttner, "Integrated THz technology for label-free genetic diagnostics," *Appl. Phys. Lett.*, vol. 80, no. 1, pp. 154–156, Jan. 2002.

[12] M. Brucherseifer, M. Nagel, P. H. Bolivar, H. Kurz, A. Bosserhoff, and R. Büttner, "Label-free probing of the binding state of DNA by time-domain terahertz sensing," *Appl. Phys. Lett.*, vol. 77, no. 24, pp. 4049–4051, Dec. 2000.

[13] J. F. O'Hara, R. Singh, I. Brener, E. Smirnova, J. Han, A. J. Taylor, and W. Zhang, "Thin-film sensing with planar terahertz metamaterials: Sensitivity and limitations," *Opt. Exp.*, vol. 16, no. 3, pp. 1786–1795, Jan. 2008.

[14] S. Vegesna, Y. Zhu, A. Bernussi, and M. Saed, "Terahertz two-layer frequency selective surfaces with improved transmission characteristics," *IEEE Trans. THz Sci. Technol.*, vol. 2, no. 4, pp. 441–448, Jul. 2012.

[15] A. Melo, A. Gobbi, M. Piazzetta, and A. da Silva, "Cross-shaped terahertz metal mesh filters: Historical review and results," *Adv. Opt. Tech.*, vol. 2012, 2012, Art. ID 530512.

[16] R. Dickie, R. Cahill, V. Fusco, H. S. Gamble, and N. Mitchell, "THz frequency selective surface filters for earth observation remote sensing instruments," *IEEE Trans. THz Sci. Technol.*, vol. 1, no. 2, pp. 450–461, Nov. 2011.

[17] V. Nazmov, E. Reznikova, Y. Mathis, J. Mathuni, A. Müller, P. Rudych, A. Last, and V. Saile, "Bandpass filters made by LIGA for the THZ region: Manufacturing and testing," *Nucl. Instrum. Meth. Phys. Res. Sect. A*, vol. 603, no. 1–2, pp. 150–152, May 2009.

[18] X. Shang, M. L. Ke, Y. Wang, and M. J. Lancaster, "WR-3 band waveguides and filters fabricated using SU8 photoresist micromachining technology," *IEEE Trans. THz Sci. Technol.*, vol. 2, no. 6, pp. 629–637, Nov. 2012.

[19] CST Microwave Studio. Darmstadt, Germany, CST GmbH, 2006.
[20] K. D. Möller, J. Warren, J. B. Heaney, and C. Kotecki, "Cross-shaped bandpass filters for the near- and mid-infrared wavelength regions," *Appl. Opt.*, vol. 35, no. 31, pp. 6210–6215, Nov. 1996.
[21] C. Debus and P. H. Bolivar, "Frequency selective surfaces for high sensitivity terahertz sensing," *Appl. Phys. Lett.*, vol. 91, Oct. 2007, Art. ID 184102.
[22] K. D. Möller, K. R. Farmer, D. V. Ivanov, O. Sternberg, K. P. Stewart, and P. Lalanne, "Thin and thick cross shaped metal grids," *Infr. Phys. Tech.*, vol. 40, no. 6, pp. 475–485, Dec. 1999.
[23] J. D. Williams and W. Wang, "Study on the postbaking process and the effects on UV lithography of high aspect ratio SU-8 microstructures," *J. Microlith., Microfab., Microsys.*, vol. 3, pp. 563–568, Oct. 2004.
[24] B. Yang, R. S. Donnan, R. Dubrovka, and W. Tang, "Negative permeability characterization of gyrotropic Hexaferrite in the millimeter wave band for engineering of double-negative devices," *J. Appl. Phys.*, vol. 109, May 2011, Art. ID 104505.
[25] J. Hong and M. J. Lancaster, *Microstrip Filters for RF/Microwave Applications*. New York, NY, USA: Wiley, 2001.

**Yi Wang** (M'09–SM'12) was born in Shandong, China. He received the B.Sc. degree in physics and M.Sc. degree in condensed matter physics from the University of Science and Technology, Beijing, China, in 1998 and 2001, respectively, and the Ph.D. degree in electronic and electrical engineering from The University of Birmingham, Edgbaston, Birmingham, U.K., in 2005.

He started his career as a Research Fellow in 2004 with The University of Birmingham, working on high-frequency device applications of novel materials and structures, including superconductors, ferroelectric materials, meta-materials, and MEMS. In 2011, he became a Senior Lecturer with the University of Greenwich, Chatham Maritime, Kent, U.K., teaching electromagnetic theory, antennas, and microwave engineering. His main research interests are millimeter-wave/terahertz devices for metrology, communications and sensors, microwave circuits based on multiport filtering networks, and antennas for medical applications. His other interests include micromachining, millimeter-wave measurements, and material characterizations.

**Bin Yang** received the B.S. degree from Beijing University of Posts and Telecommunications, Beijing, China, in 2001, and the M.Sc. and Ph.D. degrees in electronic engineering from Queen Mary University of London, London, U.K., in 2004 and 2008, respectively.

He had two years of telecommunication industrial working experience as a Technical Consultant with Fiberhome Telecommunications Ltd. and an International Business Engineer with CINTel Intelligent System, Shanghai. After completing his Ph.D. work, he remained with Queen Mary University of London (QMUL), London, U.K., as a Postdoctoral Researcher and joined the University of Bolton, Bolton, U.K., as a Lecturer in September 2013. His research areas include millimeter-wave (mm-wave) and terahertz measurement systems, mm-wave/terahertz applications in material, biology and chemistry sciences, electronic circuits, radio frequency and mm-wave technologies for healthcare and wellbeing, microwave metamaterials, and antenna and radio propagations in both soft and solid condensed materials.

**Yingtao Tian** received the Ph.D. degree in mechanical engineering from Loughborough University, Loughborough, U.K., in 2010.

His doctoral research focused on miniaturization of microelectronics, advanced electrochemical fabrication and precise manufacturing. After working on fabrication of terahertz circuits for two years as a Research Fellow with the University of Birmingham, he is currently a Research Associate with the Department of Materials, University of Manchester, Manchester, U.K. His present research interests are advanced processing of light alloys for aerospace applications.

**Robert S. Donnan** was born in Sydney, Australia, in 1967. He received the B.Sc. degree in mathematical physics from the University of Wollongong, Wollongong, Australia, in 1990, the M.Sc. degree in applied physics from the University of Technology, Sydney, Australia, in 1995, and the Ph.D. degree in solid-state physics from the University of Wollongong in 2000.

He is currently a Senior Lecturer with the School of Electronic Engineering and Computer Science, Queen Mary University of London, London, U.K. He is the founder of the Terahertz Laboratory within the School's Antennas and Electromagnetics Group, and its research interests are metrology of antenna and quasi-optical feed systems, dielectric materials, and development of terahertz metrology for the life sciences.

Dr. Donnan is a Chartered Physicist and a member of the U.K. Institute of Physics.

**Michael J. Lancaster** (SM'04) was born in England in 1958. He received the B.Sc. degree in physics and Ph.D. degree from Bath University, Bath, U.K., in 1980 and 1984, respectively.

His doctoral research focused on nonlinear underwater acoustics. After leaving Bath University, he joined the Surface Acoustic Wave (SAW) Group, Department of Engineering Science, Oxford University, Oxford, U.K., as a Research Fellow. The research was in the design of new, novel SAW devices, including filters and filter banks. In 1987, he became a Lecturer with The University of Birmingham, Birmingham, U.K., in the Department of Electronic and Electrical Engineering, lecturing in electromagnetic theory and microwave engineering. Shortly after he joined the department, he began the study of the science and applications of high-temperature superconductors, working mainly at microwave frequencies. He was promoted to head of the Emerging Device Technology Research Centre in 2000 and head of the Department of Electronic, Electrical and Computer Engineering in 2003. He has published two books and over 170 papers in refereed journals. His present personal research interests include microwave filters and antennas, as well as the high-frequency properties and applications of a number of novel and diverse materials.

Prof. Lancaster is Fellow of the IET and U.K. Institute of Physics. He is a Chartered Engineer and Chartered Physicist. He has served on the IEEE Microwave Theory and Techniques (MTT) IMS technical committee.